



**HAL**  
open science

## Early-stage growth of GeTe on Si(111)-Sb

Boris Croes, Fabien Cheynis, Yannick Fagot-Revurat, Pierre Müller, Stefano Curiotto, Frédéric Leroy

► **To cite this version:**

Boris Croes, Fabien Cheynis, Yannick Fagot-Revurat, Pierre Müller, Stefano Curiotto, et al.. Early-stage growth of GeTe on Si(111)-Sb. *Physical Review Materials*, 2023, 7 (1), pp.014409. 10.1103/PhysRevMaterials.7.014409 . hal-04184850

**HAL Id: hal-04184850**

**<https://hal.science/hal-04184850>**

Submitted on 22 Aug 2023

**HAL** is a multi-disciplinary open access archive for the deposit and dissemination of scientific research documents, whether they are published or not. The documents may come from teaching and research institutions in France or abroad, or from public or private research centers.

L'archive ouverte pluridisciplinaire **HAL**, est destinée au dépôt et à la diffusion de documents scientifiques de niveau recherche, publiés ou non, émanant des établissements d'enseignement et de recherche français ou étrangers, des laboratoires publics ou privés.

# Early-stage growth of GeTe on Si(111)-Sb

B. Croes,<sup>1</sup> F. Cheynis,<sup>1</sup> Y. Fagot-Revurat,<sup>2</sup> P. Müller,<sup>1</sup> S. Curiotto,<sup>1</sup> and F. Leroy<sup>1</sup>

<sup>1</sup>*Aix Marseille Univ, CNRS, CINAM, AMU-TECH, Marseille, France*

<sup>2</sup>*Univ Lorraine, CNRS, IJL, F-54000 Nancy, France*

(Dated: December 16, 2022)

The advent of germanium telluride as a promising ferroelectric Rashba semiconductor for spintronic applications requires the growth of nanometer-thick films of high crystalline quality. In this study, we have elucidated the initial growth stages of GeTe on Si(111)-Sb by scanning tunneling microscopy and low energy electron diffraction. We demonstrate the presence of an initial 0.35 nm-thick GeTe buffer layer followed by the 2D growth of GeTe *via* Frank-Read sources of atomic steps. As shown by core level spectroscopy, Sb is acting as a surfactant during growth up to a 5 nm-thick film. X-ray diffraction, transmission electron microscopy and low energy electron microscopy evidence that numerous mirror domains and in-plane misorientations appear early in the growth process and are gradually buried at the film/substrate interface. The use of a miscut Si substrate close to Si(111) allows suppressing these defects since the early beginning of growth.

Among ferroelectrics, a new class of materials with high potentialities for spintronic applications has been introduced and known as ferroelectric Rashba semiconductors [1]. In this context  $\alpha$ -GeTe exhibits spin-polarized electronic states with the largest Rashba parameter currently reported. Considerable effort has been devoted to the experimental characterization of its electronic band structure [2–5]. Major results have been obtained on  $\alpha$ -GeTe thin films. It has been demonstrated the reversal of the ferroelectric polarization under an electric field [6] and a consistent change of the spin chirality of the band structure [7 and 8]. Even more fascinating GeTe thin films have shown remarkable transport properties at RT such as non-reciprocal charge transport [9] or ferroelectric switching of the spin-to-charge conversion [10]. All these results take advantage of the ferroelectric property of the  $\alpha$ -GeTe phase. This phase has a rhombohedral structure (space group R3m) and bulk Curie temperature well above RT ( $T_c \sim 650 - 700$  K). The spontaneous polarization of  $\alpha$ -GeTe is along the pseudocubic  $\langle 111 \rangle$  leading to the formation of 4 ferroelastic variants. Different substrates have been used to grow GeTe thin films, Si(001) [11 and 12], Si(111) [30], Si(111)-H [14], Si(111)-Sb [15], BaF<sub>2</sub>(111) [16 and 17] or InP(111) [8]. As reported by Wang et al. [15]  $\alpha$ -GeTe thin films with a quasi-single crystalline quality can be grown on Si(111) by molecular beam epitaxy using a pre-deposition of 1 monolayer of Sb onto the substrate. Despite a significant lattice mismatch of  $\sim 8.5\%$  with the reconstructed substrate, the GeTe layer is relaxed since the very beginning of growth. Croes et al. [18] have shown that GeTe thin films thinner than 30 nm have a unique polarization state perpendicular to the film surface. This single polarization state provides the opportunity to address the persistence of ferroelectricity in nanometer-thick films and its fundamental relationship with the spin texture and transport properties. However the growth process of GeTe thin films has been overlooked in the low thickness regime. *In situ* reflection high energy electron diffraction (RHEED) measurements have shown that GeTe thin films are crystalline since the beginning of growth [19]. It has also

been shown, by Raman spectroscopy, that the rhombohedral distortion of  $\alpha$ -GeTe occurs at  $\sim 0.7$  nm of deposition through the Peierls distortion [19]. Complementary measurements by atomic force microscopy have suggested that the surface of a 2 nm-thick GeTe film exhibits a smooth two-dimensional morphology [15]. However the growth mechanisms in the nanometer-thick film regime are still unknown as well as the nature and density of defects. Their understanding and control are crucial in the context of GeTe thin film optimization with respect to future spintronic-based applications.

In this article we address the structure and morphology of GeTe thin films during the very first stages of growth on Si(111)-Sb. Using scanning tunneling microscopy (STM) we show that GeTe thin films grow initially *via* a homogeneous and crystalline buffer layer. Then atomically flat 2D islands of GeTe nucleate and grow preferentially at Si step edges with a typical size of 50 nm at  $T=275^\circ\text{C}$ . For a 0.7 nm-thick film, an interfacial relaxation mechanism occurs *via* threading dislocations (Frank-Read sources) that promotes a layer-by-layer growth mode. This process is rapidly dominated by a step-flow growth mode of GeTe layers. Despite a high quality of the surface morphology, a significant amount of mirror domains and in-plane misorientations between adjacent grains is evidenced by low energy electron diffraction (LEED) and dark-field low energy electron microscopy (LEEM). These defects are buried close to the interface with the Si substrate and strongly decay with the film thickness. An alternate growth method using a miscut silicon substrate successfully suppresses these defects.

## I. EXPERIMENTAL SECTION

Si(111) wafers (Siltronix; 550  $\mu\text{m}$  -thick;  $\rho=1-10 \Omega\text{cm}$ ) are first cleaned by acetone and ethanol rinsing before introduction in ultra-high vacuum (UHV,  $10^{-8}$  Pa). Then the substrates are degassed at 1000 K during 12 h followed by repeated high temperature annealing (1500 K)

85 during a few minutes in order to obtain a clean  $7\times 7$  143 material S2 [21])  
 86 surface reconstruction. The substrate surface and sub-  
 87 sequent growth are characterized by *in situ* RHEED  
 88 (figure 1). First a deposition of 1 monolayer of Sb is  
 89 performed on the Si(111) surface, forming the so-called  
 90 Si(111)- $\sqrt{3}\times\sqrt{3}$ -Sb reconstruction that greatly improves  
 91 the crystalline quality of the GeTe film [15]. The GeTe  
 92 thin films are grown by co-deposition of Ge (1175 °C)  
 93 and Te (310 °C) in UHV on a sample maintained at  
 94 275°C. In these conditions the flux ratio between Ge:Te is  
 95 fixed at 2:5 in order to compensate the high desorption  
 96 rate of Te [12]. All the deposition sources are effusion  
 97 cells from MBE-Komponenten GmbH. After growth, the  
 98 samples are transferred under UHV conditions thanks  
 99 to a homemade transfer suitcase and characterized by  
 100 scanning tunneling microscopy (STM) with a VT-STM  
 101 (Scienta Omicron GmbH), by LEEM and LEED using  
 102 a LEEM III microscope (Elmitec GmbH). STM images  
 103 were obtained at room temperature in constant current  
 104 mode with typical imaging conditions ( $U=-1$  V,  $I= 20$   
 105 pA, W tip). LEED patterns were measured at 16 eV and  
 106 26 eV incident electron energies. To quantify the presence  
 107 of mirror domains, LEED and dark-field LEEM images of  
 108 the GeTe surface are performed at 26 eV incident electron  
 109 energy where a high contrast is achieved. The internal  
 110 structure of thick GeTe films ( $>40$  nm) has been studied  
 111 by X-ray diffraction at BM32 beamline (ESRF) and  
 112 TEM. X-ray diffraction data have been measured at 18  
 113 keV [ $\lambda=0.06888$  nm] with a beam size of  $200\times 300\ \mu\text{m}^2$   
 114 and collected onto a 2D detector. The data have been  
 115 converted from the detector coordinates (pixel index) to  
 116 diffraction angles and then to reciprocal space coordi-  
 117 nates. The 3D reciprocal space maps have been visual-  
 118 ized using the ParaView software. TEM investigations  
 119 were performed using  $[1\bar{1}0]$  zone axis at an accelerating  
 120 voltage of 300 kV on a JEOL JEM-3010 instrument with  
 121 a spatial resolution of 0.17 nm. Using focused ion beam  
 122 preparation procedure (Dual beam FIB, FEI Helios 600  
 123 NanoLab), electron transparent ultra-thin sections were 144  
 124 extracted from the thin films of GeTe on Si. The typi-  
 125 cal dimensions of the electron transparent ultrathin sec-  
 126 tions are  $15\ \mu\text{m}$  (length)  $\times 5\ \mu\text{m}$  (height)  $\times 150\text{--}200$  nm  
 127 (thickness). Considering surface chemical composition,  
 128 core level photoemission peaks were measured at CAS-  
 129 SIOPEE beamline (Synchrotron SOLEIL, France) using  
 130 a 800 eV incident photon energy. A typical energy res-  
 131 olution of around 100 meV is achieved, using a Scienta  
 132 R4000 electron-analyzer with a 0.5 mm entrance slit and  
 133 a pass-energy of 100 eV. To protect the GeTe surface  
 134 from contamination during sample transfer to SOLEIL  
 135 synchrotron UHV chamber, a Te capping was used. The  
 136 capping is removed in UHV first by a mild Ar ion bom-  
 137 bardment at RT (1 keV, 10  $\mu\text{A}$ ) to remove the top most  
 138 oxidized layers then by annealing at 220 °C to desorb the  
 139 complete Te layer (see supplementary material S1 [20]).  
 140 Apart from structural, morphological and chemical as-  
 141 pects the GeTe thick film quality has also been checked  
 142 with respect to electric conductivity (see supplementary

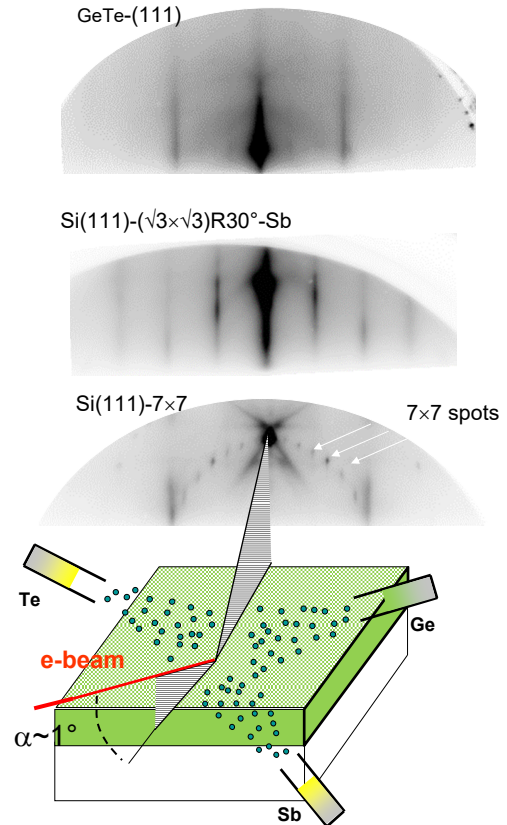


FIG. 1. Experimental protocol of GeTe growth. RHEED patterns of Si(111)- $7\times 7$  surface (bottom), Si(111)- $\sqrt{3}\times\sqrt{3}$ -Sb reconstruction (middle) and GeTe thin film of 3 nm thickness (top).

## 145 II. RESULTS AND DISCUSSION

### 146 A. Initial growth of GeTe thin film

146 The surface morphology of a 0.35 nm-thick GeTe film  
 147 (1 bilayer of bulk  $\alpha$ -GeTe) grown on Si(111)- $\sqrt{3}\times\sqrt{3}$ -  
 148 Sb surface shows a homogeneous grainy aspect [figure  
 149 2(a)]. This layer will be called the buffer layer. The  
 150 measured step height on the surface is 0.31 nm and cor-  
 151 responds to the atomic step height of the Si(111) surface  
 152 [figure 2(b)]. Despite the granular aspect of the GeTe  
 153 layer a crystalline order occurs as shown by LEED [fig-  
 154 ure 2(c)]. The main diffraction peaks of GeTe are per-  
 155 fectly aligned with Si diffraction peaks. This indicates  
 156 a preferential epitaxy such that GeTe(111) $\parallel$ Si(111) and  
 157 GeTe $[1\bar{1}0]\parallel$ Si $[1\bar{1}0]$  in pseudocubic coordinates [15]. The  
 158 measured in-plane lattice parameter mismatch between  
 159 Si and GeTe is  $8.3\%\pm 2.5\%$  [figure 2(e)]. Therefore the in-  
 160 plane lattice parameter of GeTe is  $0.416\pm 0.010$  nm con-  
 161 sidering that the interatomic distance between Si atoms is

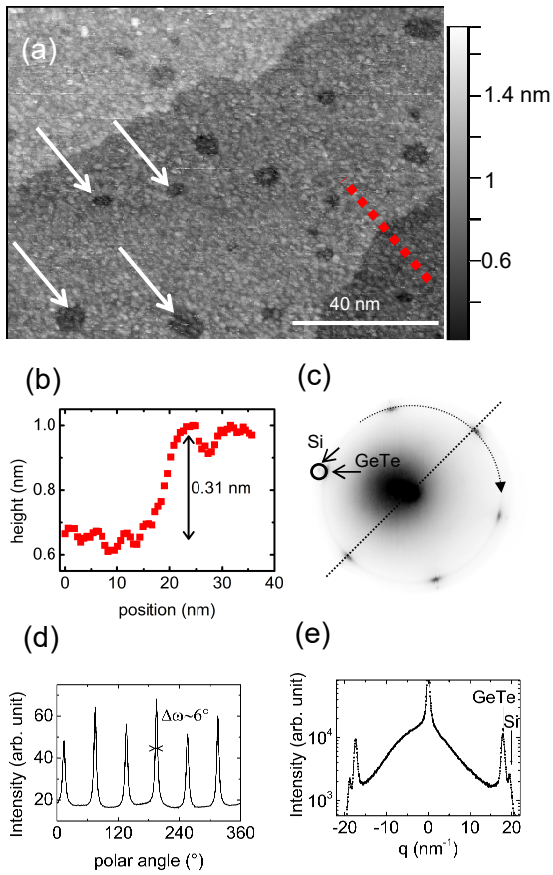


FIG. 2. (a) STM image of a 0.35 nm-thick (1 BL) GeTe thin film grown on Si(111)- $\sqrt{3} \times \sqrt{3}$ -Sb. Holes on Si(111) terraces (white arrows). (b) Height profile across a step edge [red dotted line in (a)]. The step height is 0.31 nm. (c) LEED at incident electron energy  $E = 16$  eV showing the Si substrate and the GeTe layer diffraction patterns. (d) Polar plot of the intensity of the LEED pattern at GeTe peak radial coordinate [dotted arrow in (c)]. The full width at half maximum of the spots is  $\Delta\omega \sim 6^\circ$ . (e) Radial plot of the intensity of the LEED pattern [dashed dark line in (c)]. The GeTe and Si peaks are shown by arrows.

172  $a_{Si} = 0.384$  nm. This value is close to the expected lattice  
 162 parameter of bulk  $\alpha$ -GeTe considering a rhombohedron  
 163 axis normal to the surface. Thus the GeTe film is relaxed  
 164 since the very first atomic bilayer (BL) [19]. However  
 165 some disorder is observed: significant in-plane misorien-  
 166 tations (FWHM  $\sim 6^\circ$ ) and a diffuse scattering ring are  
 167 evidenced by LEED [figure 2(c)-(d)]. In addition figure  
 168 2(a) shows a few monoatomic holes of 5-10 nm diameter  
 169 on the substrate. These holes indicate that a part of the  
 170 Si substrate atoms are consumed during the initial GeTe  
 171 growth.

173 Figure 3(a) shows the STM image of a sample where  
 174 the GeTe growth has been stopped when the scattering  
 175 rods of the RHEED pattern of GeTe become thinner and  
 176 well-defined ( $\sim 0.7$  nm, 2 BLs). We observe atomically  
 177 flat islands on the surface explaining the occurrence of

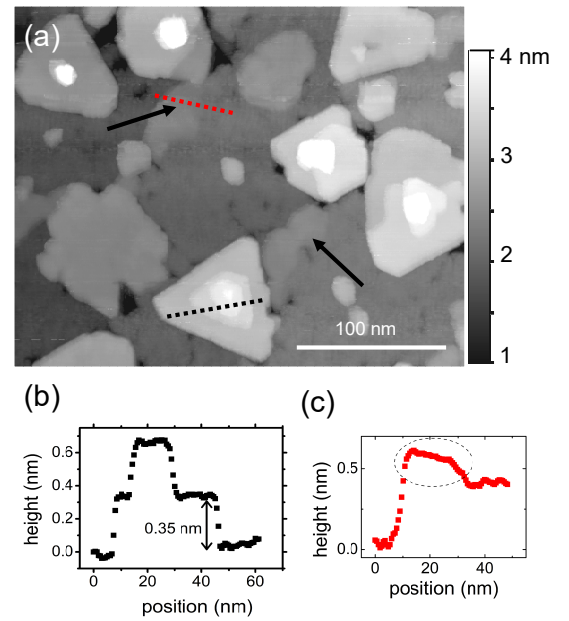


FIG. 3. (a) STM image of a GeTe thin film of 2 BL, *i.e.* when RHEED scattering rods are intense and well-defined. Black arrows: areas of smooth height variations of the surface morphology. (b) Height profile taken across step-edges (black dotted line on a GeTe island). The step height is 0.35 nm as expected for GeTe. (c) Height profile taken across the red dotted line of (a) showing a smooth height variation on the upper terrace (see red dashed oval region).

178 thin and elongated RHEED scattering rods (the buffer  
 179 layer is still present in between islands). The islands nu-  
 180 cleate preferentially at Si step edges and the step height  
 181 on the islands is now 0.35 nm as expected for a GeTe  
 182 BL [figure 3(b)]. The step edges of the Si substrate are  
 183 strongly disturbed by the growth. It is a clear indica-  
 184 tion that the topmost Si atoms are mobile at the onset  
 185 of growth. The Si mobility could result from the high  
 186 tendency of alloying between Ge and Si as well as Te and  
 187 Si. In addition, at some places close to step edges, the  
 188 topography shows smooth height variations over  $\sim 10$  nm  
 189 lateral distance that are accompanied with a change of  
 190 the surface aspect: flat/uphill and more grainy/downhill  
 191 [see black arrows in figure 3(a) and height profile in fig-  
 192 ure 3(c)]. These local changes of the surface height could  
 193 be a signature of a local activation of the Peierls dis-  
 194 tortion that was hindered for a 0.35 nm-thick film [19].  
 195 However we cannot exclude that these variations arise  
 196 from composition inhomogeneities that may involve the  
 197 silicon substrate and/or Sb (see supplementary materials  
 198 S3 [22]).

199 Upon a GeTe deposition of 1 nm ( $\sim 3$  BL), STM image  
 200 in figure 4(a) shows that extended and smooth islands are  
 201 already formed on the whole surface. The growth is not  
 202 a perfect layer-by-layer growth since new layers appear  
 203 before the previous layer is complete. This observation  
 204 corroborates the rapid decrease of the amplitude of the

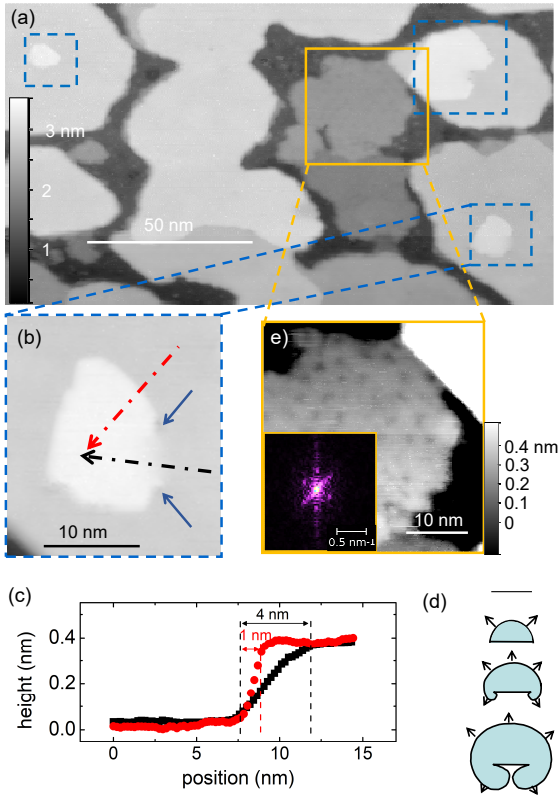


FIG. 4. (a) STM image of a 1 nm-thick (3 BL) GeTe thin film grown on Si(111)- $\sqrt{3} \times \sqrt{3}$ -Sb ( $U = -1V$ ;  $I = 20$  pA). Dashed blue squares show Frank-Read source of dislocations. (b) Close view of a Frank-Read source of dislocations from (a). Blues arrows indicate the location of the two threading dislocations. (c) Height profiles along the dashed arrows in (b). The black height profile is located in between two threading dislocations with opposite Burger vectors and show a smooth height variation ( $\sim 4$  nm width). The red height profile passes across an abrupt step edge (resulting from one threading dislocation). (d) Scheme of the evolution during growth of a Frank-Read source of dislocations (surface steps). (e) Close view of a surface area showing a modulated surface topography (orange areas in (a)). Inset: Fourier transform of the morphology showing an ordered hexagonal lattice.

205 RHEED oscillations as shown by Wang and coworkers  
 206 [19]. In addition to the layer-by-layer growth mode, we  
 207 can also notice that the surface has some very distinctive  
 208 surface steps consisting of curved step edges with both  
 209 ends terminated by a threading dislocation (see figures  
 210 4(a)-(b)). To reach the top of the corresponding islands,  
 211 two different paths can be considered: one path with  
 212 an abrupt height variation (step edge) and another path  
 213 with a smooth height increase over 4 nm [figure 4(c)].  
 214 The net displacement of both paths normal to the sur-  
 215 face is 0.35 nm, *i.e.* equal to the height of a bilayer. This  
 216 indicates that the threading dislocations are screw-like.  
 217 In NaCl compounds, such as GeTe (considering a pseudo-  
 218 cubic lattice) and for a (111) crystallographic plane, the  
 219 Burgers vector of dislocations is usually  $\frac{1}{2}[110]$ , corre-

220 sponding to the measured height displacement [23]. In  
 221 this case two screw dislocations with opposite Burger vec-  
 222 tors are formed that cancel the total normal displacement  
 223 on the surface [figures 4(b)-(c)]. These structures can be  
 224 referred as Frank-Read [24] sources of dislocations and  
 225 generate surface steps [figure 4(d)]. We can also distin-  
 226 guish Moiré-like patterns on terraces [figure 4(e)]. The  
 227 Fourier transform of the STM image shows a hexagonal  
 228 like pattern with a lattice period of  $p = 0.26 \pm 0.05$  nm $^{-1}$ .  
 229 This pattern can be associated with a hexagonal super-  
 230 lattice of period  $a = \frac{1}{p} \times \frac{2}{\sqrt{3}} = 4.4 \pm 1.0$  nm. Since the  
 231 in-plane lattice parameter mismatch between bulk GeTe  
 232 and Si is  $\frac{\Delta a}{a_{Si}} = 8.3 \pm 2.5\%$ , then the expected coincidence  
 233 lattice of the relaxed layer of GeTe(111) on Si(111)-Sb  
 234 with GeTe[ $1\bar{1}0$ ] || Si[ $1\bar{1}0$ ] has a period of 4.64 nm [15].  
 235 This value matches the periodicity of the Moiré pattern.  
 236 This coincidence lattice is also in adequation with the  
 237 misfit dislocation network that as been characterized by  
 238 HR-TEM at the GeTe/Si interface of thicker films by  
 239 Croes and coworkers [18].

240 Already for the deposition of a 2 nm-thick GeTe film  
 241 (6 BL), extended atomically flat terraces ( $> 50$  nm)  
 242 are present on the whole surface [figure 5-(a)]. As the  
 243 RHEED intensity of the specular beam reaches a steady  
 244 state behaviour [19] we can consider that the growth  
 245 proceeds *via* a step flow mode. Adjacent terraces may  
 246 be separated by slight depressions arising from the grain  
 247 boundaries due to the local lattice mismatch. The step  
 248 edge profiles show a 0.35 nm height as expected for a  
 249 GeTe bilayer [see inset of figure 5-(a)]. Some few remain-  
 250 ing surface steps are still arising *via* Frank-Read sources  
 251 of dislocations [see dashed squares in figure 5-(a)]. As un-  
 252 derlined in a similar system, PbTe(111) grown on BaF $_2$   
 253 [25], their disappearance could result from the annihila-  
 254 tion of the dislocations pair due to their strong attractive  
 255 interaction and assuming an increase of the dislocation  
 256 mobility with the film thickness. We can also notice that  
 257 the island step edges are smooth. For a GeTe film several  
 258 tens of nanometers thick, two types of step edges exist:  
 259 the straight step edge called A-step and the notched one  
 260 called B-step [figure 5-(b)]. As underlined by Croes et  
 261 al. [26] the occurrence of notches at the B-step edges  
 262 neutralizes the electric charges. The absence of trian-  
 263 gular notches for nanometer-thick GeTe thin films could  
 264 result from the intermixing with the Sb layer deposited  
 265 prior GeTe deposition that may stabilize the step edge  
 266 structure. The overall growth of GeTe on Si(111) as a  
 267 two dimensional film suggests that the surface energy of  
 268 GeTe(111) is smaller than the difference between the sur-  
 269 face energy of Si(111) and GeTe/Si interfacial energy. As  
 270 calculated by Deringer and coworkers [27] the surface en-  
 271 ergy of the Te-terminated surface of GeTe(111) is 2.1  
 272 eV/nm $^2$  and the Si(111) surface energy is 9.2 eV/nm $^2$   
 273 [28]. The latter energy is reduced by 1.8 eV/nm $^2$  consid-  
 274 ering the Sb adsorption at the surface [29]. Since GeTe  
 275 wets perfectly the Si substrate, these energies allow es-  
 276 timating a maximum value for the interfacial energy of  
 277 GeTe/Si  $9.2 - 1.8 - 2.1 = 5.3$  eV/nm $^2$ .

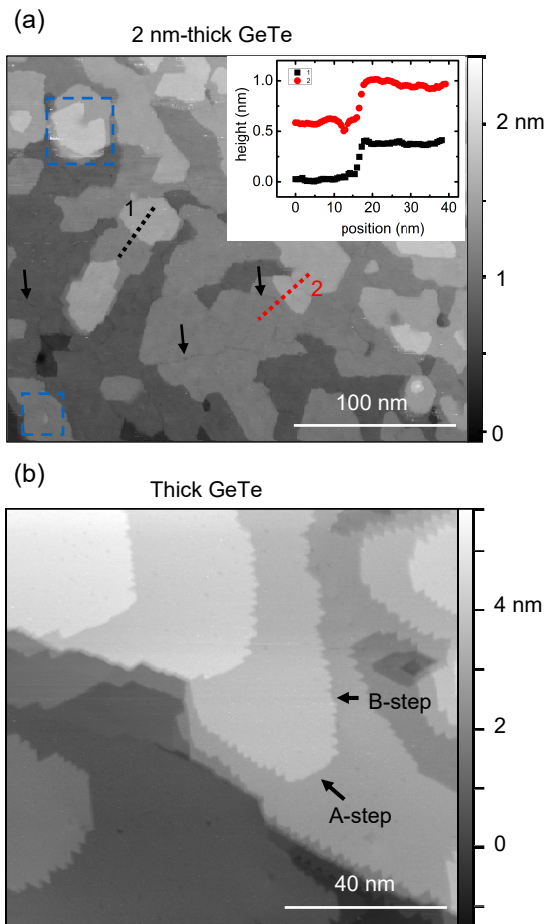


FIG. 5. (a) Large scale STM image of a 2 nm-thick GeTe thin film grown on Si(111)- $\sqrt{3} \times \sqrt{3}$ -Sb ( $U = -1V$ ;  $I = 20 \text{ pA}$ ). Slight depressions at grain boundaries (black arrows). Remaining Frank-Read sources of dislocations (dashed blue squares). Inset: bilayer step-edges. (b) STM image of a 40 nm-thick GeTe film showing notched step-edges (B-step) and smooth step-edges (A-step).

## 278 B. Sb surfactant role, mosaicity and mirror 279 domains

280 To address the chemical composition of the film dur-  
281 ing the initial stages of GeTe growth, we have made XPS  
282 measurements at Sb 3d and Te 3d binding energies con-  
283 sidering an incident photon energy of 800 eV. Sb con-  
284 tributions ( $3d_{3/2}$  and  $3d_{5/2}$ ) can be seen on the XPS  
285 spectrum for a 2-nm thick GeTe film [figure 6-(a)]. By  
286 increasing the XPS sensitivity to the sample surface, in-  
287 creasing the exit angle of detection of the photo-emitted  
288 electrons with respect to the surface normal, we see that  
289 the Te 3d peaks nearly vanish while the intensity of Sb  
290 peaks increases. This result shows that a significant  
291 amount of Sb is located in the surface region. To rule  
292 out possible photodiffraction effects we have made mea-  
293 surements at two incident angles ( $25^\circ$  and  $30^\circ$ ). For a 5  
294 nm-thick film, the Sb peak still shows a faint contribu-

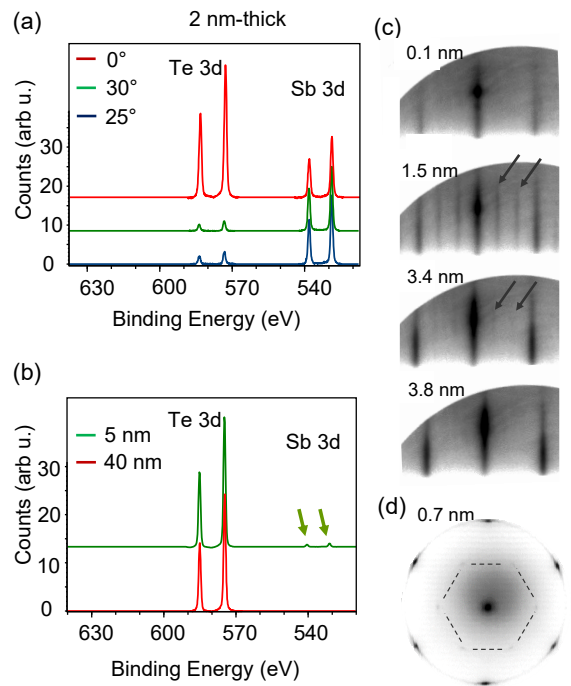


FIG. 6. (a) XPS spectra of a 2 nm-thick GeTe film at different exit angles of photo-emitted electrons. (b) XPS spectra of a 5 nm- and a 40 nm-thick GeTe films at  $0^\circ$  exit angle. The arrows show the Sb  $3d_{3/2}$  and Sb  $3d_{5/2}$  peaks of the 5 nm-thick sample. (c) RHEED patterns at the beginning of the growth of GeTe: from 0.1 nm to 3.8 nm deposited film. Arrows point to additional rods that appear a few tens of seconds after the beginning of the growth and disappear a few minutes later. (d) LEED pattern for a 0.7 nm-thick GeTe thin film. Si(111)- $\sqrt{3} \times \sqrt{3}$ -Sb reconstruction (dashed hexagon).

295 tion and it is completely absent for a 40 nm-thick film  
296 [figures 6-(b)]. Therefore Sb is progressively buried in-  
297 side the GeTe film during growth. In addition to spec-  
298 troscopy the presence of Sb at the surface is correlated  
299 with the occurrence of additional peaks on the RHEED  
300 and LEED patterns [figures 6-(c)-(d)]. Those peaks can  
301 be attributed to a  $\sqrt{3} \times \sqrt{3}$  reconstruction of the GeTe  
302 surface [15]. The reconstruction is visible up to a  $\sim 4$  nm-  
303 thick GeTe layer that is close to the detection limit of Sb  
304 by XPS indicating that the reconstruction is promoted  
305 by the presence of Sb at the surface. In addition this  
306 reconstruction is not detected when GeTe is grown on  
307 Si(111) without the deposition of 1 monolayer of Sb [30].  
308 Therefore the presence of Sb favors the layer-by-layer and  
309 step flow growth modes by acting as a surfactant during  
310 the early stages of growth. This result is corroborated  
311 by previous studies on the surfactant effect of Sb, *e.g.*  
312 during growth of Ge layers on Si(111) [31 and 32]. The  
313 favorable termination of the growing layer with Sb at the  
314 growth front prevents the formation of islands to relax  
315 the elastic stress due to the lattice mismatch. In such  
316 surfactant-mediated epitaxy a complete relaxation of the  
317 interface *via* misfit dislocations is favored [33 and 34].



318 We can infer that a similar mechanism is occurring in  
319 the case of GeTe growth on Si(111)-Sb.

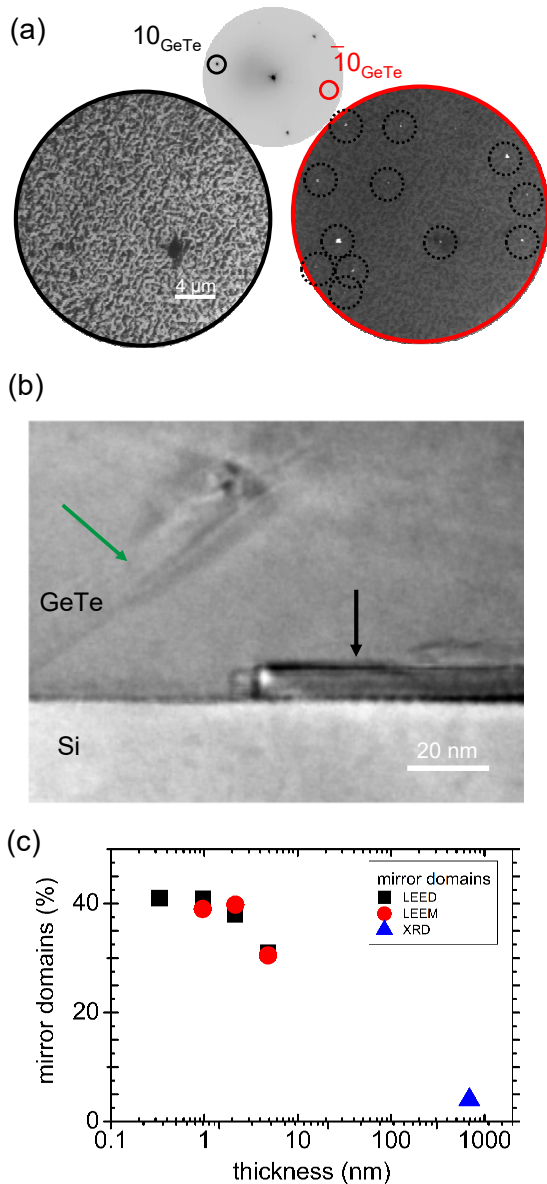


FIG. 7. (a) Dark-field LEEM images of a 460 nm-thick GeTe film measured with 26 eV electron incident energy and using 10 (left image) and  $\bar{1}0$  (right image) GeTe spots. The LEED pattern is in the middle (above). Due to the threefold symmetry of the GeTe crystalline structure, a strong intensity difference between 10 and  $\bar{1}0$  occurs. The intensity difference is maximum for 26 eV energy incident electrons. The mirror domains are detected using the  $\bar{1}0$  LEED spot for imaging using 26 eV electrons (dark dashed circles in right image). (b) TEM cross-section of a 200 nm-thick GeTe film. The black arrow points to a mirror domain buried at the interface with silicon. The green arrow shows a ferroelectric nanodomain crossing the GeTe film (see also [18]). (c) Evolution of the fraction of mirror domains with film thickness as measured by LEED and LEEM (below 5 nm) and X-ray diffraction (> 40 nm).

320 To evaluate the crystalline quality of nanometer-thick  
321 GeTe film we have characterized the evolution of the frac-  
322 tion of mirror domains (ACB stacking instead of ABC)  
323 and in-plane misorientation (mosaicity). For a 460 nm-  
324 thick GeTe film, the LEED pattern shows sharp diffrac-  
325 tion spots demonstrating that the mosaicity is below  $1^\circ$   
326 (figure 7-(a) and [26]). In addition LEEM images using  
327 dark-field imaging mode on major and minor diffraction  
328 peaks show that only a very small fraction of mirror do-  
329 mains can be detected. These results are confirmed by  
330 TEM [see figure 7-(b)]. For nanometer-thick GeTe thin  
331 films, the fraction of mirror domains have been measured  
332 by LEED. Indeed the LEED pattern at 26 eV shows six  
333 diffraction spots at  $60^\circ$  and a threefold symmetry consid-  
334 ering the peak intensities. Therefore the mirror domain  
335 ratio can be estimated by measuring the intensity ratio  
336 between two peaks at  $60^\circ$  called 10 and  $\bar{1}0$  using 26 eV  
337 incident electrons. We deduce that there is about 41% of  
338 mirror domains for a 0.28 nm-thick film, and this value  
339 decreases to  $\sim 31\%$  for a 2.8 nm-thick film [figure 7-(c)].  
340 Considering a large range of film thickness studied by  
341 X-ray diffraction and LEED we can deduce that the mir-  
342 ror domain ratio drops with the film thickness [see figure  
343 7-(c)]. Even though the initial GeTe film has a signif-  
344 icant amount of defects, they are rapidly buried at the  
345 interface with the Si substrate [see TEM image in figure  
346 7-(b)]. At the beginning of growth, the fraction of mirror  
347 domains is slightly below one half indicating that GeTe is  
348 able to interact with the 3-fold symmetry of the substrate  
349 [15]. However the strongest effect seems to be related to  
350 the kinetics of growth that allows the main domain to  
351 rapidly bury the mirror domains. Considering the mo-  
352 saicity of the GeTe films, the 3D reciprocal space map of  
353 a 200 nm-thick GeTe film around a non-symmetric Bragg  
354 peak  $202_h$  [see figure 8-(a)] shows a slight in-plane mi-  
355 sorientation of  $1.2^\circ$  (FWHM= $0.5 \pm 0.1^\circ$  for a 800 nm-thick  
356 sample). We can also notice that 3 additional peaks are  
357 found nearby the main GeTe peak. They arise due to the  
358 presence of GeTe ferroelastic domains [18]. The in-plane  
359 broadening of the Bragg peaks show that the misorienta-  
360 tions also impact the ferroelastic domains and the mirror  
361 domains [see figure 8-(b)]. For nanometer-thick GeTe  
362 thin films, the mosaicity has been measured by LEED  
363 (see supplementary materials S4 [36]). The low energy  
364 electron scattering ring measured for a 0.28 nm-thick film  
365 (0.8 bilayer) begins to disappear at the second bilayer  
366 (0.7 nm) and is not present at the fourth bilayer (1.4  
367 nm). The polar plot of the full width at half maximum  
368 of the diffraction peaks shows that the misorientation de-  
369 creases with the film thickness from  $5.8^\circ \pm 0.2^\circ$  to  $4.7^\circ$   
370  $\pm 0.2^\circ$  respectively for 0.28 and 2.8 nm-thick films [figure  
371 8-(c)]. Considering a large range of film thickness stud-  
372 ied by X-ray diffraction and LEED we can see that the  
373 in-plane misorientation decreases with the film thickness  
374 [see figure 8-(c)]. To suppress the mirror domains and  
375 misorientations between adjacent grains since the begin-  
376 ning of growth we have used Si substrates slightly miscut  
377 with respect to Si(111). The vicinal Si(556) substrate is  
378

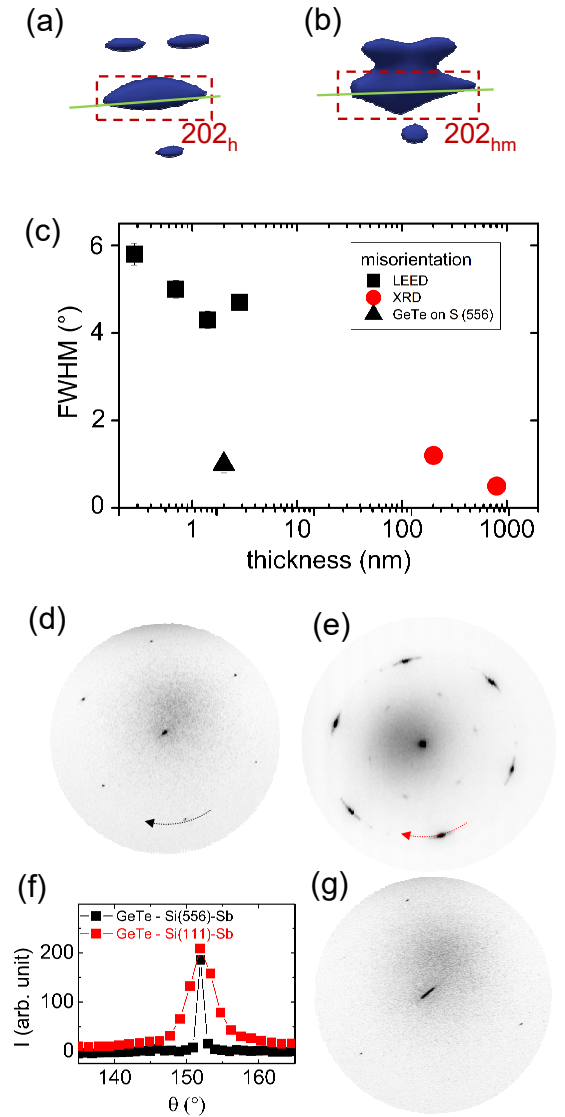


FIG. 8. (a)-(b) 3D reciprocal space maps of GeTe  $202_h$  and GeTe  $202_{hm}$  Bragg peaks of GeTe thin film grown on Si(111)-Sb and obtained by X-ray diffraction (200 nm-thick sample).  $h$  stands for hexagonal unit cell of the main GeTe domain and  $hm$  for the mirror domains. Around the main Bragg peaks, additional spots arise due to the presence of ferroelastic domains [18 and 35]. The Bragg peaks are elongated in-plane due to a residual in-plane mosaicity of the GeTe film. (c) Evolution of the in-plane mosaicity (full width at half maximum) with the film thickness as measured by LEED (below 5 nm) and X-ray diffraction (> 40 nm). (d) LEED pattern of a 2 nm-thick GeTe thin film grown on Si(556)-Sb. Incident electron energies: 16 eV. (e) LEED pattern of a 1.4 nm-thick GeTe thin film grown on Si(111)- $\sqrt{3} \times \sqrt{3}$ -Sb. Incident electron energy: 16 eV. (f) Polar plots along the LEED diffraction peaks from GeTe grown on Si(556)-Sb [see image (d)] and Si(111)-Sb [see image (e)]. (g) LEED pattern of a 2 nm-thick GeTe thin film grown on Si(556)-Sb. Incident electron energies: 26 eV. The pattern has a clear 3-fold symmetry.

379 tilted by  $5^\circ$  with respect to the (111) plane in the  $[\bar{1}\bar{1}2]$   
 380 direction. Figures 8-(d)-(e) show a comparison between  
 381 the LEED patterns with 16 eV incident electrons of GeTe  
 382 ultrathin films grown on Si(556)-Sb and on Si(111)-Sb.  
 383 Very sharp diffraction spots are measured on the miscut  
 384 substrate and the  $\sqrt{3} \times \sqrt{3}$ -Sb is absent. This result in-  
 385 dicates that the misorientations are strongly suppressed  
 386 [below  $1^\circ$ , see figure 8-(f)]. In addition the LEED pat-  
 387 tern, using 26 eV incident electrons, of the GeTe ultrathin  
 388 film grown on the miscut substrate shows a very strong  
 389 asymmetry of intensity between two adjacent peaks at  
 390  $60^\circ$  [figure 8-(g)]. This result clearly indicates that mir-  
 391 ror domains are also suppressed. We can thus assess that



- 422 <sup>1</sup> D. Di Sante, P. Barone, R. Bertacco, and S. Picozzi, Elec- 483  
423 tric Control of the Giant Rashba Effect in Bulk GeTe, Adv. 484  
424 Mater., 25, 509 (2013).
- 425 <sup>2</sup> M. Liebmann, C. Rinaldi, D. Di Sante, J. Kellner, C. Pauly, 485  
426 R. N. Wang, J. E. Boschker, A. Giussani, S. Bertoli, M. 486  
427 Cantoni, L. Baldrati, M. Asa, I. Vobornik, G. Panaccione, 487  
428 D. Marchenko, J. Sánchez-Bariga, O. Rader, R. Calarco, 488  
429 S. Picozzi, R. Bertacco, and M. Morgenstern, Giant 489  
430 Rashba-Type Spin Splitting in Ferroelectric GeTe(111) 490  
431 Adv. Mater., 28, 560 (2016).
- 432 <sup>3</sup> J. Krempaský, S. Muff, F. Bisti, M. Fanciulli, H. Volfová, 491  
433 A. P. Weber, N. Pilet, P. Warnicke, H. Ebert, J. Braun, 492  
434 F. Bertran, V. V. Volobuev, J. Minár, G. Springholz, 493  
435 J. H. Dil, and V. N. Strocov, Entanglement and manipu- 494  
436 lation of the magnetic and spin-orbit order in multiferroic 495  
437 Rashba semiconductors Nat. Commun., 7, 13071 (2016).
- 438 <sup>4</sup> J. Krempaský, H. Volfová, S. Muff, N. Pilet, G. Landolt, 496  
439 M. Radovic, M. Shi, D. Kriegner, V. Holý, J. Braun, 497  
440 H. Ebert, F. Bisti, V. A. Rogalev, V. N. Strocov, 498  
441 G. Springholz, J. Minár, and J. H. Dil, Disentangling bulk 499  
442 and surface Rashba effects in ferroelectric  $\alpha$ -GeTe, 500  
443 Phys. Rev. B, 94, 205111 (2016).
- 444 <sup>5</sup> G. Kremer, T. Jaouen, B. Salzmänn, L. Nicolaï, M. Rumo, 501  
445 C. W. Nicholson, B. Hildebrand, J. H. Dil, J. Minár, 502  
446 G. Springholz, J. Krempaský, C. Monney, Unveiling the 503  
447 complete dispersion of the giant Rashba split surface states 504  
448 of ferroelectric  $\alpha$ -GeTe(111) by alkali doping, Phys. Rev. 505  
449 Research 2, 033115 (2020).
- 450 <sup>6</sup> A. V. Kolobov, D. J. Kim, A. Giussani, P. Fons, J. Tominaga, 506  
451 R. Calarco, and A. Gruverman, Ferroelectric switching 507  
452 in epitaxial GeTe films, APL Mater., 2, 066101 (2014).
- 453 <sup>7</sup> C. Rinaldi, S. Varotto, M. Asa, J. Slawinska, J. Fujii, 508  
454 G. Vinai, S. Cecchi, D. Di Sante, R. Calarco, I. Vobornik, 509  
455 G. Panaccione, S. Picozzi, and R. Bertacco, Ferroelectric 510  
456 Control of the Spin Texture in GeTe, Nano Lett. 18, 2751 511  
457 (2018).
- 458 <sup>8</sup> J. Krempaský, S. Muff, J. Minar, N. Pilet, M. Fanciulli, 512  
459 A. P. Weber, E. B. Guedes, M. Caputo, E. Mueller, 513  
460 V. V. Volobuev, M. Gmitra, C. A. F. Vaz, V Scagnoli, 514  
461 G. Springholz, and J. H. Dil, Operando Imaging of All- 515  
462 Electric Spin Texture Manipulation in Ferroelectric and 516  
463 Multiferroic Rashba Semiconductors, Phys. Rev. X 8, 517  
464 021067 (2018).
- 465 <sup>9</sup> Y. Li, Y. Li, P. Li, B. Fang, X. Yang, Y. Wen, D.-X. Zheng, 518  
466 C.-H. Zhang, X. He, A. Manchon, Z.-H. Cheng, and X.-X. 519  
467 Zhang, Nonreciprocal charge transport up to room tem- 520  
468 perature in bulk Rashba semiconductor  $\alpha$ -GeTe, Nat. 521  
469 Commun. 12, 540 (2021).
- 470 <sup>10</sup> Sara Varotto, Luca Nessi, Stefano Cecchi, Jagoda Slawinska, 522  
471 Paul Noel, Simone Petro, Federico Fagiani, Alessandro 523  
472 Novati, Matteo Cantoni, Daniela Petti, Edoardo Al- 524  
473 bisetti, Marcio Costa, Raffaella Calarco, Marco Buon- 525  
474 giorno Nardelli, Manuel Bibes, Silvia Picozzi, Jean- 526  
475 Philippe Attane, Laurent Vila, Riccardo Bertacco, and 527  
476 Christian Rinaldi, Room-temperature ferroelectric switch- 528  
477 ing of spin-to-charge conversion in germanium telluride, 529  
478 Nature electronics 4, 740 (2021).
- 479 <sup>11</sup> A. V. Kolobov, P. Fons, M. Krbal, J. Tominaga, A. Giussani, 530  
480 K. Perumal, H. Riechert, R. Calarco, T. Uruga, Local 531  
481 structure of epitaxial GeTe and Ge<sub>2</sub>Sb<sub>2</sub>Te<sub>5</sub> films grown on 532  
482 InAs and Si substrates with (100) and (111) orientations: 533  
483 An x-ray absorption near-edge structure study, J. Appl. 534  
484 Phys. 117, 125308 (2015)
- 485 <sup>12</sup> Karthick Perumal, Epitaxial growth of Ge-Sb-Te based 535  
486 phase change materials, PhD thesis, Humboldt-Universität 536  
487 zu Berlin, Mathematisch-Naturwissenschaftliche Fakultät 537  
488 I (2013).
- 489 <sup>13</sup> Alessandro Giussani, Karthick Perumal, Michael Hanke, 538  
490 Peter Rodenbach, Henning Riechert, Raffaella Calarco, On 539  
491 the epitaxy of germanium telluride thin films on silicon 540  
492 substrates, Physica Status Solidi B 249, 1939 (2012).
- 493 <sup>14</sup> Jamo Momand, Jos E. Boschker, Ruining Wang, Raffaella 541  
494 Calarco, Bart J. Kooi, Tailoring the epitaxy of Sb<sub>2</sub>Te<sub>3</sub> and 542  
495 GeTe thin films using surface passivation, CrystEngComm 543  
496 20,340 (2018).
- 497 <sup>15</sup> R. Wang, J. E. Boschker, E. Bruyer, D. Di Sante, 544  
498 S. Picozzi, K. Perumal, A. Giussani, H. Riechert, and 545  
499 R. Calarco, Toward Truly Single Crystalline GeTe Films: 546  
500 The Relevance of the Substrate Surface, J. Phys. Chem. 547  
501 C 118, 29724 (2014).
- 502 <sup>16</sup> R. T. Lechner, G. Springholz, M. Hassan, H. Groiss, R. 548  
503 Kirchschlager, J. Stangl, N. Hrauda, G. Bauer, Phase separa- 549  
504 tion and exchange biasing in the ferromagnetic IV–VI 550  
505 semiconductor Ge<sub>1-x</sub>Mn<sub>x</sub>Te, Applied Physics Letters 97, 551  
506 023101 (2010).
- 507 <sup>17</sup> M. Hassan, G. Springholz, R. T. Lechner, H. Groiss, 552  
508 R. Kirchschlager, G. Bauer, Molecular beam epitaxy of 553  
509 single phase GeMnTe with high ferromagnetic transition 554  
510 temperature, J. Cryst. Growth 323, 363 (2011).
- 511 <sup>18</sup> B. Croes, F. Cheynis, Y. Zhang, C. Voulot, K. D. 555  
512 Dorkenoo, S. Cherifi-Hertel, C. Mocuta, M. Texier, T. Cor- 556  
513 nelius, O. Thomas, M.-I. Richard, P. Müller, S. Curiotto, 557  
514 and F. Leroy, Ferroelectric nanodomains in epitaxial GeTe 558  
515 thin films, Phys. Rev. Materials 5, 124415 (2021).
- 516 <sup>19</sup> Ruining Wang, Davide Campi, Marco Bernasconi, Jamo 559  
517 Momand, Bart J. Kooi, Marcel A. Verheijen, Matthias 560  
518 Wuttig, and Raffaella Calarco, Ordered peierls distortion 561  
519 prevented at growth onset of GeTe ultra-thin films, Sci. 562  
520 Rep. 6, 32895 (2016).
- 521 <sup>20</sup> See Supplemental Material S1 at [publisher address] for 563  
522 LEED measurements before and after Te desorption. 564
- 523 <sup>21</sup> See Supplemental Material S2 at [publisher address] for 565  
524 electric conductivity measurements of GeTe thin film as 566  
525 function of temperature. 567
- 526 <sup>22</sup> See Supplemental Material S3 at [publisher address] for 568  
527 XPS dataset around Si core level binding energies. 569
- 528 <sup>23</sup> John Price Hirth and Jens Lothe, Theory of Dislocations, 570  
529 Krieger Publishing Company (1992).
- 530 <sup>24</sup> F. C. Frank and W. T. Read, Multiplication Processes for 571  
531 Slow Moving Dislocations, Phys. Rev. 79, 722 (1950).
- 532 <sup>25</sup> G Springholz, AY Ueta, N Frank, and G Bauer, Spiral 572  
533 growth and threading dislocations for molecular beam epi- 573  
534 taxy of PbTe on BaF<sub>2</sub>(111) studied by scanning tunneling 574  
535 microscopy, Appl. Phys. Lett. 69, 2822 (1996).
- 536 <sup>26</sup> B. Croes, F. Cheynis, P. Müller, S. Curiotto, and F. Leroy, 575  
537 Polar surface of ferroelectric nanodomains in GeTe thin 576  
538 films, Phys. Rev. Materials 6, 064407 (2022).
- 539 <sup>27</sup> V. L. Deringer, M. Lumeij, and R. Dronskowski, Ab Initio 577  
540 Modeling of  $\alpha$ -GeTe(111) Surfaces, J. Phys. Chem. C 578  
541 116, 15801 (2012).
- 542 <sup>28</sup> R. Zhachuk, J. Coutinho, A. Dolbak, V. Cherepanov, and 579  
543 B. Voigtländer, Si(111) strained layers on Ge(111): Evi-

- 544 dence for  $c(2 \times 4)$  domains, *Phys. Rev. B* 96, 085401 (2017). 566
- 545 <sup>29</sup> H. Guesmi, L. Lapena, G. Tréglia, and P. Müller, Cover- 567
- 546 age dependence of Sb/Si(111) adsorption and desorption 568
- 547 modes: Interplay between chemical interactions and site 569
- 548 transitions, *Phys. Rev. B* 77, 085402 (2008). 570
- 549 <sup>30</sup> Alessandro Giussani, Karthick Perumal, Michael Hanke, 571
- 550 Peter Rodenbach, Henning Riechert, and Raffaella 572
- 551 Calarco, On the epitaxy of germanium telluride thin films 573
- 552 on silicon substrates, *Phys. Status Solidi B* 249, 1939 574
- 553 (2012). 575
- 554 <sup>31</sup> M. Hornvohogen, F. K. Legoues, M. Copel, M. C. 576
- 555 Reuter, R. M. Tromp, Defect self-annihilation in 577
- 556 surfactant-mediated epitaxial growth, *Phys. Rev. Lett.* 67, 578
- 557 1130 (1991). 579
- 558 <sup>32</sup> B. Voigtländer, and A. Zinner, Surfactant mediated epi- 580
- 559 taxy of Ge on Si(111): The role of kinetics and charac- 581
- 560 terization of the Ge layers, *Journal of Vacuum Science &* 582
- 561 *Technology A* 12, 1932 (1994). 583
- 562 <sup>33</sup> G. Meyer, B. Voigtländer, and N.M. Amer, Scanning tun- 584
- 563 neling microscopy of surfactant-mediated epitaxy of Ge on 585
- 564 Si(111): strain relief mechanisms and growth kinetics, *Sur- 586*
- 565 face Science 274, L541 (1992).
- <sup>34</sup> G. Meyer, B. Voigtländer, and N.M. Amer, Strain-relief 587
- mechanism in surfactant-grown epitaxial germanium films 588
- on Si(111), *Phys. Rev. B* 44, 12894 (1991).
- <sup>35</sup> D. Kriegner, G. Springholz, C. Richter, N. Filet, 589
- E. Mueller, M. Capron, H. Berger, V. Holy, J. H. Dil, and 590
- J. Krempasky, Ferroelectric Self-Poling in GeTe Films and 591
- Crystals, *Crystals* 9, 335 (2019). 592
- <sup>36</sup> See Supplemental Material S4 at [publisher address] for 593
- LEED patterns and polar plots as function of film thick- 594
- ness. 595
- <sup>37</sup> Eugenio Zallo, Stefano Cecchi, Jos E. Boschker, Anto- 596
- nio M. Mio, Fabrizio Arciprete, Stefania Privitera, and 597
- Raffaella Calarco, Modulation of van der Waals and clas- 598
- sical epitaxy induced by strain at the Si step edges in GeS- 599
- bTe alloys, *Sci. Rep.* 7, 1466 (2017). 600
- <sup>38</sup> Fabrizio Arciprete, Jos Emiel Boschker, Stefano Cecchi, 601
- Eugenio Zallo, Valeria Bragaglia, and Raffaella Calarco, 602
- Hints for a General Understanding of the Epitaxial Rules 603
- for van der Waals Epitaxy from Ge-Sb-Te Alloys, *Adv.* 604
- Mater. Interfaces* 9, 2101556 (2022). 605